

pubs.acs.org/JPCA Article

Detailed Study of the Formation of Soot Precursors and Soot in Highly Controlled Ethylene(/Toluene) Counterflow Diffusion Flames

Published as part of The Journal of Physical Chemistry virtual special issue "Combustion in a Sustainable World: From Molecules to Processes".

Kevin Gleason and Alessandro Gomez*



Cite This: J. Phys. Chem. A 2023, 127, 276-285



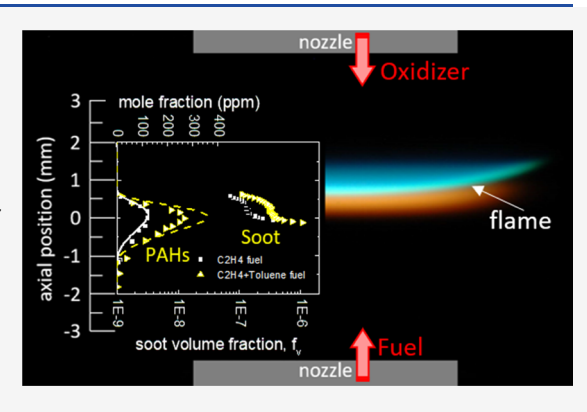
ACCESS

III Metrics & More

Article Recommendations

Supporting Information

ABSTRACT: We perform spatially resolved measurements of temperature, gaseous species up to three-ring Polycyclic Aromatic Hydrocarbons (PAHs), and soot in atmospheric pressure counterflow diffusion flames. First, we characterize fully a baseline ethylene flame and then a toluene-seeded flame in which an aliquot of ethylene in the feed stream is replaced with 3500 ppm of prevaporized toluene. The goal is twofold: to investigate the impact of a common reference fuel component of surrogates of transportation fuels and bypass the main bottleneck to soot formation from aliphatic fuels, that is, the formation of the first aromatic ring. The composition of the fuel and oxidizer streams are adjusted to maintain a constant stoichiometric mixture fraction and global strain rate, thereby ensuring invariance of the temperature—time history in the comparison between the two flames and decoupling the chemical effects of the fuel



substitution from other factors. Major combustion products and critical radicals are fixed by the baseline flame, and profiles of critical C2-C5 species precursors to aromatic formation are invariant in both flames. On the other hand, doping with toluene boosts the aromatic content and soot volume fraction, increasing the mole fraction of benzenoid structures and soot volume fraction by a factor of 2 or 3, relative to the baseline ethylene flame. This finding is consistent with the expectation that the formation of the first aromatic ring is no longer a bottleneck to soot formation in the doped flame. In addition, toluene bypasses completely benzene formation, opening a radical recombination pathway to soot precursors through the production of $C_{14}H_{14}$ (via dimerization of benzyl radical) and pyrene (through dimerization of indenyl radical).

1. INTRODUCTION

The study of soot formation even in well-defined laminar flame environments retains an overwhelming complexity if one uses practical petroleum-derived fuels such as gasoline and diesel and jet fuel that are composed of hundreds of aromatic and aliphatic components.^{1,2} Studying their coupled chemical kinetic behavior would be an unrealistic challenge. The research community has been focused on the establishment of surrogate fuels, consisting of primary reference constituents that are formulated to mimic some predefined combustion performance parameters.³⁻⁵ But the formulation of surrogates is a moving target and it is more valuable to focus on reference fuel components of surrogates of transportation fuel including aliphatic species (e.g., n-heptane, iso-octane, n-decane, and ndodecane) and monoaromatic species with alkyl substitutions, such as toluene and 1,2,4-trimethylbenzene (TMB).^{6,7} The presence of aromatics in transportation fuels is known to enhance PAH and soot production, with toluene and TMB as major surrogate components dictating surrogate soot behavior.

The chemistry of toluene and TMB has been studied in various high-temperature reacting environments. $^{3,8-10}$ In particular, there is a rising interest in studying Polycyclic Aromatic Hydrocarbon (PAH) and soot formation of surrogates including binary and ternary mixtures, $^{11-24}$ to investigate the effect of strain rate, 19 stoichiometric mixture fraction, 11,12,19 and pressure 24 in flames. Kruse et al. 19 studied the effect of strain rate and stoichiometric mixture fraction on soot formation in counterflow diffusion flames using n-heptane, iso-octane, and toluene individually, as three gasoline surrogate components. Ethylene is the most commonly used aliphatic fuel in soot investigations and its chemical behavior is therefore relatively well understood. Even so, models that accurately predict soot

Received: September 13, 2022 Revised: November 29, 2022 Published: December 21, 2022





formation in ethylene flames overpredict the soot load in gasoline surrogate flames by 1 to 2 orders of magnitude, suggesting room for improvement in the chemistry of practical fuels and their surrogates. Park et al. 16 investigated the same three surrogate components as in ref 19 in counterflow diffusion flames, exploring the synergistic effect of binary and ternary mixtures on PAH chemistry and soot formation. As the toluene ratio increased, the PAH concentration (LIF signal) and soot volume fraction (LII signal) increased. The model developed therein was able to capture the synergistic effect of *n*-heptane/ toluene and iso-octane/toluene mixtures. However, these investigations kept constant the oxygen content as the mixture ratios were varied. So, an increase in the toluene ratio systematically increased the stoichiometric mixture fraction in both the *n*-heptane/toluene and iso-octane/toluene mixtures. Since the PAH concentration and volume fraction are sensitive to the changes in the stoichiometric mixture fraction, 19 it is difficult to differentiate synergistic effects from mixture fraction effects.

In addition to soot measurements, the characterization of a flame structure is necessary to validate chemistry models predicting the formation of PAHs and soot. 11,18,23,25,26 One method to isolate the kinetic pathways of different fuels is to seed trace amounts of the fuel of interest into a baseline flame. The rationale is that the baseline flame provides a well-defined environment which is used to control temperature—time history and fixes major combustion products and critical radicals (H, O, OH). 11,14,27 In previous work in our laboratory, Carbone and Gomez studied nonsooting and incipiently sooting counterflow diffusion flames doped with either toluene 1 or 1,2,4-trimethylbenzene (TMB), 1 focusing on major species and the formation of the one- and two-ring aromatic species. They observed that the C3 and C4 pathways were not accurately captured by two kinetic mechanisms, pointing out a need for improvement of aromatic ring opening mechanism.

The quantification of species larger than benzene is helpful to define critical pathways of PAH growth and the relative importance of Hydrogen Abstraction Carbon Addition (HACA),²⁸ PAH radical recombination, or radical chain reactions.^{29–32} However, the precursors to benzene are equally important for validating the cyclization of aliphatic parent fuels and the ring opening mechanism for aromatic parent fuels. Therefore, it is ideal to track quantitatively the *entire* evolution from parent fuel to PAHs and eventually soot in a single flame environment.

We perform a comprehensive analysis on the influence of toluene, a common aromatic component of surrogates of transportation fuels, on soot formation in atmospheric pressure counterflow diffusion flames with excellent control of the temperature—time history by fixing the global strain rate and stoichiometric mixture fraction.^{33–35} To isolate the effect of the aromatic on soot formation, we characterize fully first a baseline ethylene flame and then a toluene-seeded flame in which an aliquot of ethylene in the feed stream is replaced with prevaporized toluene. We perform spatially resolved measurements of temperature, gaseous species up to three-ring PAHs, and soot volume fraction. Regardless of surrogate considerations, the replacement of an aliphatic with an aromatic compound has significance at a fundamental level: it should result in the removal of the potential bottleneck that aliphatic fuels experience in their evolution to soot, that is, the formation of the very first aromatic ring.³⁶ During pyrolysis toluene retains

its aromatic structure and accelerates the formation of multiring PAHs via aromatic radical recombination. 8,9,14,18,21,30,31,37

The present study revisits toluene doping of an ethylene flame that had already been the subject of work in our laboratory ¹¹ for multiple reasons: (i) implementing a much greater control of the flame by fixing global strain rate and stoichiometric mixture fraction, thereby enabling the comparison of two flames with a constant temperature—time history and decoupling the chemical effects of the fuel substitution from other factors; (ii) introducing position-dependent corrections in the spatial profiles to account for flame dragging, using a finer thermocouple and relying on two-dimensional modeling to prescribe accurate velocity boundary conditions, ³⁸ which results in a drastically improved agreement between experiments and modeling; and (iii) expanding the species database to include three-ring aromatics like phenanthrene, which is beneficial to models for validation of kinetic mechanisms, and soot volume fraction.

From a broader perspective, the importance of understanding soot formation is twofold. First, the transition to a sustainable world will take several decades and we will not be able to wean ourselves off fossil fuels for a long time. Projections from multiple sources, including the U.S. Energy Information Administration, still list fossil fuels as the dominant source of energy in 2050, although in a diminished capacity compared to today's energy landscape. This statement holds true especially for certain sectors like power production in aviation and maritime applications, in which petroleum-based liquid fuels such as jet fuel and diesel are likely to remain dominant players. More generally, soot is not only a byproduct of combustion in power generation but also a natural product in forest fires, whose frequency and intensity are increasing as a result of global warming.

Second, the approach highlighted in the present article relies on a combination of suitably corrected intrusive sampling and chemical analysis of combustion intermediates and soot precursors, as well as on optical measurements of soot in laminar flames, with complementary use of computational modeling with detailed chemistry. This quantitative approach, integrated with additional diagnostics for the comprehensive characterizations of the distributions of mass, size, elementary charge state, and chemical (including radical) functionalities of precursors and soot in incipiently sooting flames is likely to remain the most promising means to shed light on this very challenging research area.

2. METHODS

2.1. Experimental Diagnostics. Burner Geometry and Flame Selection. The burner consists of two identical converging nozzles oriented in counterflow configuration. The internal diameter of each nozzle is 6.35 mm and the nozzles are separated by 8 mm. Both nozzles are surrounded by a nitrogen shroud to shield the flame from external disturbances. We start with a baseline incipiently sooting diffusion flame of ethylene, feeding calibrated flows of ethylene/nitrogen and oxygen/ nitrogen through the bottom and top nozzles, respectively. Momentum is unbalanced to position the flame front approximately centered between the burner nozzles, with $\rho_f V_f^2 = 1.2 \rho_{ox} V_{ox}^2$ with obvious notation, to ensure adiabatic boundary conditions and easy access for sampling/diagnostics. The counterflow configuration provides a one-dimensional flow field in the vicinity of the burner axis, as confirmed by digital camera photographs showing a locally flat flame.

The flame soot load is precisely controlled via changes in the maximum flame temperature, global strain rate, and stoichiometric mixture fraction to ensure that the soot scattering is distinguishable from that of the gas phase. This baseline flame is perturbed by replacing a small amount of ethylene with vaporized toluene and adjusting the oxidizer composition to keep constant the stoichiometric mixture fraction $Z_{st} = 0.17$ and the global strain rate $a = 70 \text{ s}^{-1} = (V_{avg,f} + V_{avg,ox})/L$ in order to preserve the temperature—time history of the baseline flame. The bottom nozzle and fuel stream is heated to 368 K to prevaporize a spray of toluene injected with a syringe pump, and the preheat treatment is applied also to the baseline flame to ensure that the boundary conditions are otherwise identical. The amount of toluene added is such that the soot load increase is distinguishable relative to the baseline flame. The difference in the computed peak flame temperature is less than 10 K, which is smaller than the experimental uncertainty. The boundary conditions of both flames are listed in Table 1, including mole fractions in the feed streams, mass averaged velocity (V_{avg}) , and axial velocity gradient, as well as measured temperature at the burner mouths.

Sampling Probe and GC. For speciation of the flame intermediates and products, we insert radially a silica capillary probe (OD/ID = 360 μ m/150 μ m). The probe is kept under vacuum to withdraw a sample from the flame as the burner is translated vertically and sample several positions along the burner axis. The sampling position is tracked by measuring with a digital camera the position of the probe tip relative to the peak blue chemiluminescence of the flame. Details of the sampling methodology are described in previous work. 38,41 The sampling line connected to the probe is heated to 423 K to prevent condensation of heavy species and the sampling line feeds directly to the injection port of a gas chromatograph/mass spectrometer system (Agilent 6890A/5973N) to analyze samples on the fly. The GC is equipped with a thermal conductivity detector, flame ionization detector, and mass spectrometer to quantify H2, O2, N2, CO, CO2, and hydrocarbons up to three-ring PAH (190 amu). All quantified species are calibrated by at least one of the following methods: gaseous

Table 1. Flame Boundary Conditions

	baseline		doped
Fuel Stream			
C_2H_4	0.375		0.371
N_2	0.625		0.625
C_7H_8	0 ppm		3500 ppm
V_{avg}		27.2 cm/s	
V_{ax}		43.43 cm/s	
dV_r/dr		23.7 s^{-1}	
T		368 K	
Oxidizer Stream			
O_2	0.238		0.241
N_2	0.762		0.759
V_{avg}		28.8 cm/s	
V_{ax}		41.25 cm/s	
dV_r/dr		40.4 s^{-1}	
T		356 K	
Flame Properties			
T_{max}	2070 K		2079 K
Z_{st}		0.17	
$a(s^{-1})$		70 s^{-1}	

calibration performed with mass flow controllers (CH₄, C₂H₄, H₂, O₂, N₂), Scotty bottles (hydrocarbons up to C4), or an electrosprayed liquid solution vaporized in a hot nitrogen stream. The error in measured concentrations is estimated at \pm 5% for C3 species and smaller and \pm 15% for species larger than C3.

Temperature. Temperature measurements are performed with a silica coated R-type thermocouple with a 50 μm diameter cylindrical bead. Standard corrections for radiative losses are applied through a convective—radiative energy balance. ⁴² When measuring in the soot forming zone, the thermocouple is quickly inserted to minimize soot deposition onto the thermocouple junction and, before reusing it at a different location, it is placed in an oxidizing environment after each measurement to burn off any soot that deposited onto the junction. The uncertainty of thermocouple measurements is estimated to be at most $\pm 2\%$ and is lower at lower temperatures.

Pyrometry. Soot volume fraction is measured via pyrometry using a Nikon D70 digital camera with a well characterized spectral response (400-700 nm) as described exhaustively in past work. Soot luminosity is measured by imaging the flame through a 210 mm focal length lens and a f/8 aperture. Images are acquired in sets of 20 at different levels of saturation to improve the overall signal-to-noise ratio in the low temperature sooting region. The flames investigated in this work are laminar and very stable, with flame flickering, as determined by the position of the flame chemiluminescence, confined to within the pixel resolution. An Abel transform deconvolves the line-of-sight images of each color channel (red, green, and blue) into two-dimensional fields and the ratio of any two Abel-transformed color channels is related to the intensity of radiation emitted through Planck's law

$$\frac{S_i}{S_j} = \frac{\int \eta_i(\lambda) \lambda^{(-5+\alpha)} \left[\exp\left(\frac{hc}{\lambda k_B T}\right) - 1 \right]^{-1} d\lambda}{\int \eta_j(\lambda) \lambda^{(-5+\alpha)} \left[\exp\left(\frac{hc}{\lambda k_B T}\right) - 1 \right]^{-1} d\lambda} \tag{1}$$

The overall optical efficiency, accounting for the detection efficiency of each color channel and transmission losses through the optics, is expressed with the wavelength dependent term $\eta(\lambda)$. The dispersion exponent, α , accounts for the soot emissivity, which is assumed to follow a power-law dependence on wavelength, $\epsilon(\lambda) \sim \lambda^{-\alpha}$. The inverse power-law dependence implies that large values of α are indicative of particles that are transparent in the visible spectrum. 44 The dispersion exponent not only is an important optical parameter, but also gives a rough indication of the soot age, since it is related to the particle hydrogen to carbon (H/C) ratio. Young (mature) soot has a large (small) H/C ratio corresponding to large (small) values of the α exponent. Since all optical and proportionality constants cancel out in eq 1, α can be evaluated using the gas phase temperature that has been measured with thermocouple measurements. The soot volume fraction is calculated using the following expression

$$f_{v} = -\frac{\lambda_{e}}{\tilde{K}_{ext}L_{p}} \ln \left\{ 1 - \epsilon_{c}(\lambda_{e}) \frac{\tau_{c}S_{s}}{\tau_{s}S_{c}} \exp \left[-\frac{hc}{k_{B}\lambda_{e}} \left(\frac{1}{T_{c}} - \frac{1}{T_{s}} \right) \right] \right\}$$
(2)

where λ_e , L_p , τ , and \tilde{K}_{ext} are the effective channel wavelength, pixel length, exposure time, and dimensionless extinction coefficient, respectively. We assume $\tilde{K}_{ext} = 5.34 \pm 2.68$; the

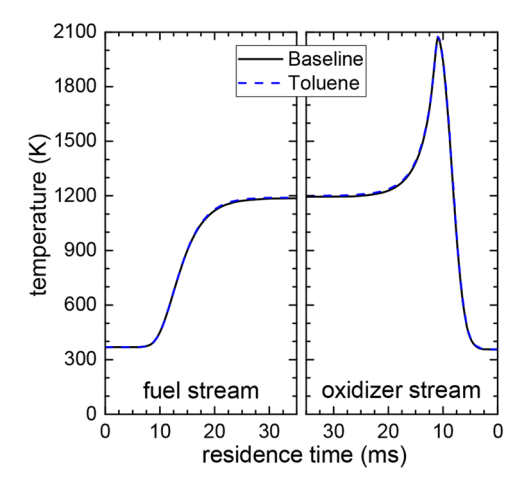


Figure 1. Calculated temperature—time history of baseline and toluenedoped flame.

variability of the extinction coefficient with wavelength and soot maturity is lumped as a general uncertainty. Subscripts "s" and "c" refer to measurements on soot particles and to a light calibration source, respectively.

2.2 Flame modeling. One-dimensional modeling of the flames is performed with ANSYS CHEMKIN-Pro⁴⁵ using the KAUST chemistry Mechanism (KM2). We account for multicomponent diffusion coefficients, thermal diffusion, and thermal radiation of CO, CO₂, H₂O, and CH₄ in the optically thin limit. The KM2 mechanism was validated in a baseline flame up to 6-ring PAH⁴⁷ and partially validated for surrogate mixtures. Two-dimensional modeling is performed in ANSYS to quantify the departure from plug flow. Briefly, we model the flow within the converging nozzle burner and shroud housing, including reactions using a simple 5-step mechanism, mixture-averaged transport, and buoyancy. The computed axial velocity (V_{ax}) and velocity gradient (dV/dz) from the 2-D simulations are provided in Table 1. The use of the simplified mechanism in

the 2-D model is to account for the flames heat release, which can influence the velocity profile at the burner exit. The 2-D simulation is identical to that described by Carbone et al., 48 except that those authors used a different software.

3. RESULTS AND DISCUSSION

Figure 1 shows the computed temperature versus the convective residence time for the two investigated flames. The residence time is calculated as the integral of the inverse axial velocity along the burner axis, with zero marking the exit of either the top or lower burner. Because the residence time approaches infinity at the stagnation plane, the fuel and oxidizer streams are plotted separately. Results show that by keeping the strain rate and stoichiometric mixture fraction constant, the addition of toluene does not affect the temperature—time history. This approach provides a useful control under conditions in which temperature-sensitive Arrhenius chemistry is operational.

Major Products, Intermediates, and Aromatics. We begin with profiles of temperature, reactants, and major combustion products in Figure 2. For all figures, the baseline flame is shown with black solid symbols and lines and the toluene-seeded flame is shown with blue open symbols and dashed lines, the lines pertaining to model predictions. The abscissa in all plots is the distance from the gas stagnation plane (GSP) with the fuel (oxidizer) stream on the left (right), represented by negative (positive) values of the axial position. The value of the stoichiometric mixture fraction places the flame on the oxidizer side of the GSP, coinciding with the position of the maximum flame temperature ($z \approx 0.8$ mm). The thermocouple measurements of the two flames are virtually identical and well reproduced by the model. Since boundary conditions on the velocity are also nearly identical, the two flames maintain a constant temperature-convective time history by design, as shown in Figure 1, by fixing the stoichiometric mixture fraction and strain rate. 34,35 As a result, any difference in flame structure caused by the addition of the aromatic fuel will be strictly chemical rather than thermal in

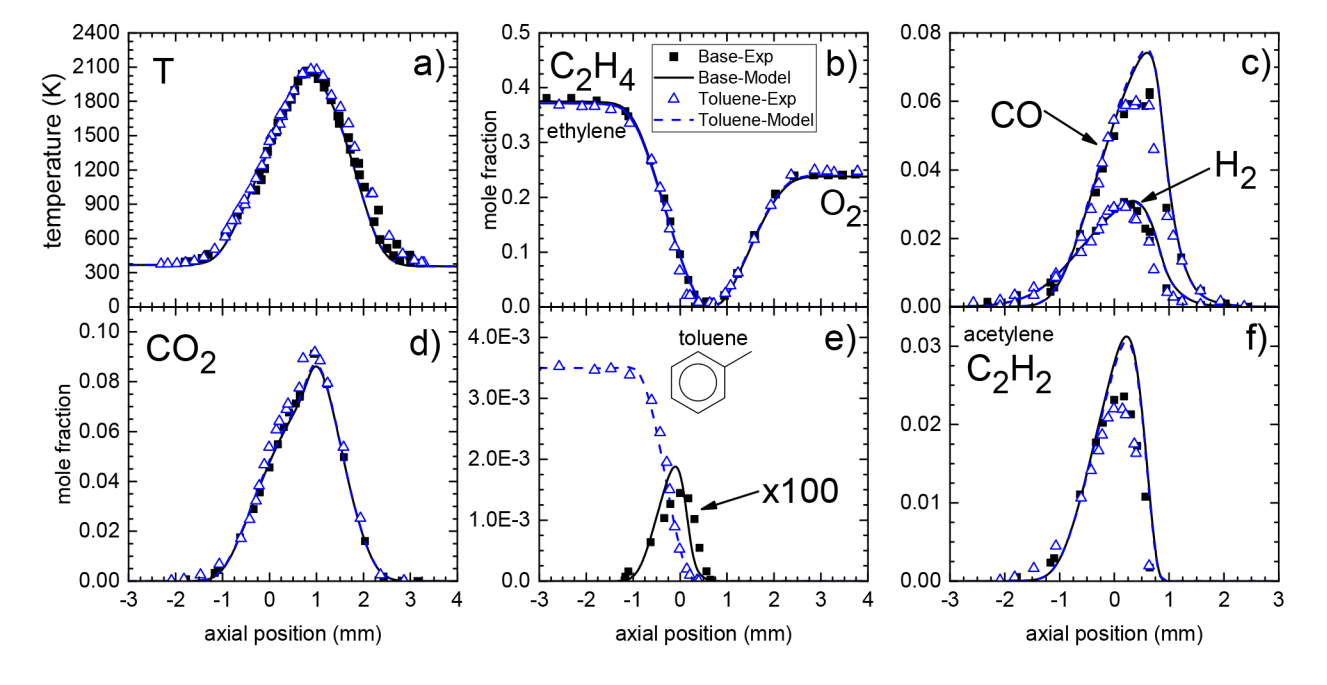


Figure 2. Profiles of temperature (a) and mole fraction of reactants and major species. The axial position is the distance from the gas stagnation plate (GSP). A factor of 100 is applied to the toluene profile in baseline flame. Symbols and lines apply also to subsequent plots in Figures 3–6.

nature. There is no discernible difference in the structure of the two investigated flames with respect to major species, with pyrolysis and oxidation of the baseline ethylene fuel as the overwhelming source of major combustion products and intermediates. 11,14 The effect of toluene-seeding (or lack thereof) is captured by the model, but CO and $\rm C_2H_2$ are overpredicted by approximately 20% and 30%, respectively. The comparison in Figure 2 confirms that the addition of toluene did not perturb significantly the baseline flame structure and allows us to focus on the effect that toluene has specifically on the chemical pathways to soot and its precursors.

We note that the quality of agreement with the model is better than in our previous work. 11 Three improvements are responsible for this outcome: the use of a finer thermocouple, the introduction of position-dependent corrections in the spatial profiles to account for flame dragging, and to a lesser extent, the use of two-dimensional modeling to prescribe accurate velocity boundary conditions by accounting for departure from plug flow and imposing both velocity and velocity gradient at the boundary³⁸ (see details in the Supporting Information). Flame "dragging" is assessed by measuring the distance from either the thermocouple junction or probe tip to the blue chemiluminescence by a digital camera. The experimental data are overlapped with the model prediction by assuming that the imaged blue chemiluminescence coincides with the location of the modeled peak mole fraction of CH*. Two-dimensional modeling quantifies the departure from plug flow, which is necessary to capture accurately the flame width and temperature-time history^{38,48} and results in minor changes in the temperature profile. Even so, such minor changes are consequential to the pyrometry measurements to be discussed later on. The present data set is also more extensive with the species database including three-ring aromatics like phenanthrene, which is beneficial for the validation of kinetic mechanisms, and the simultaneous quantification of soot.

Figure 3 shows the profiles of key aromatic compounds like benzene, naphthalene, and phenanthrene. Doping with toluene fuel boosts the aromatic content, increasing the mole fraction of each species by a constant factor of 2 to 3 relative to the baseline ethylene flame. In both flames, the peak mole fraction decreases by approximately 1 order of magnitude with each additional ring suggesting that there is a sequential growth of PAHs. ^{36,47} We observe that the detection limit is approximately 1 ppm for phenanthrene, and for this reason, we are not able to resolve the entire species profile in the baseline flame. Experiments and model are in reasonably good agreement and validate the kinetic model. We can therefore explore and compare the kinetic pathways of these three PAHs with some confidence to help identifying their role on PAH growth and soot formation.

Their production rates are shown in Figure 4 in addition to that of C_2H_2 , a key species in soot surface growth and the HACA mechanism. The vertical dashed line marks the position of the flame front. The production rate of C_2H_2 is identical in both flames, further confirming that C_2H_2 is a product of only the baseline ethylene fuel. The production rates of benzene, naphthalene, and phenanthrene are systematically higher with the addition of toluene and are shifted toward the fuel nozzle. The increase in peak production rate is consistent with the increase in peak mole fraction in Figure 3.

Benzene formation from a parent aliphatic fuel is often cited as one of the bottlenecks to aromatic/soot formation, 36 and the kinetic pathway involving C_2H_2 , C_3H_4 , C_4H_4 , etc. remains relatively unaffected in these flames because the mole fraction of

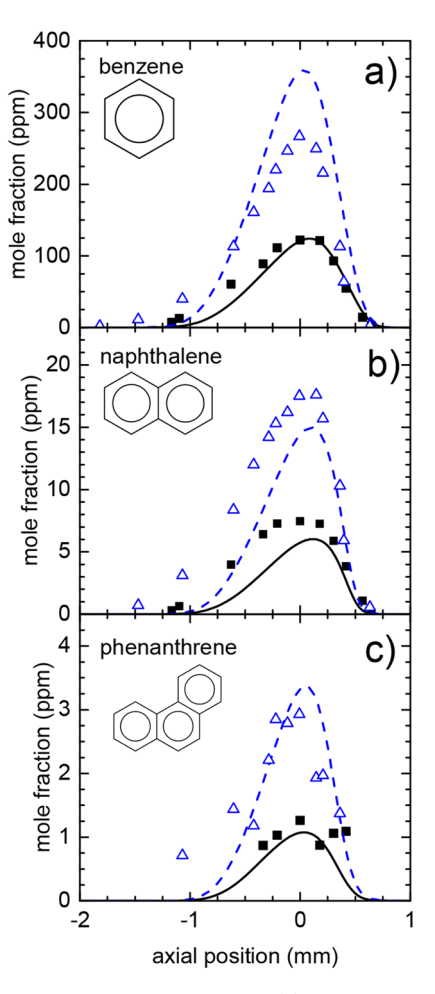


Figure 3. Mole fraction of benzene (a), naphthalene (b), and phenanthrene (c). Symbols and lines as in Figure 2.

these precursors is dictated by the pyrolytic growth of the baseline ethylene fuel. ^{11,14} Moreover, since the temperature—time history of both flames is identical, as already observed, the reaction rate constants remain fixed as well. Therefore, the addition of an aromatic fuel must, at least in part, bypasses this bottleneck of benzene formation and should directly affect the production rates of larger PAHs and possibly soot. There are nondominant pathways, such as those involving PAHs with aliphatic chains that arise from the addition of toluene as discussed below, but these species are overshadowed, in terms of both mole fraction and production rate, by the PAHs in Figures 3 and 4, and we can retain a focus on these three most abundant PAHs.

Other Precursors and Aromatics. We include, for completeness, profiles of aromatic precursors and minor aromatics in Figures 5 and 6, and all other species that were quantified are provided in the Supporting Information. Similar to the major combustion products, the C3–C5 species in Figure 5 are formed predominantly from the base ethylene fuel and their concentrations are not affected by the addition of toluene. There are two major pathways leading to the first aromatic ring (benzene) from an aliphatic fuel: propargyl radical recombination, which we can represent with the stable counterpart C_3H_4 , and the C4/C2 route. The precursors to benzene formation are unaffected by the addition of toluene, so the increase in benzene mole fraction in Figure 2 must be via pyrolysis of the toluene fuel. Cyclopentadiene (Figure 5c) is invariant in both flames, but

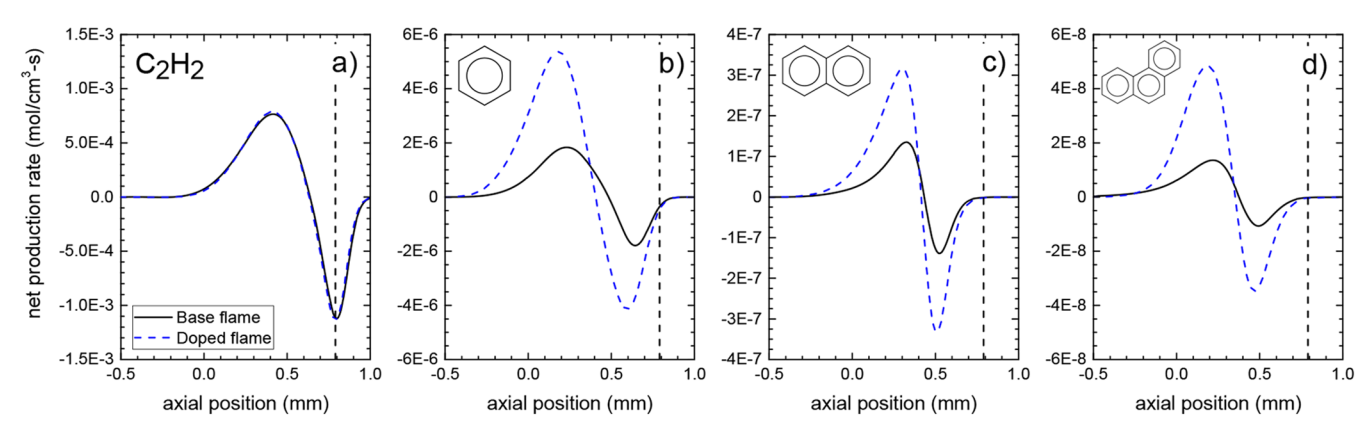


Figure 4. Computed profiles of net production rate of acetylene, benzene, naphthalene, and phenanthrene. The vertical dashed line marks the position of the flame front.

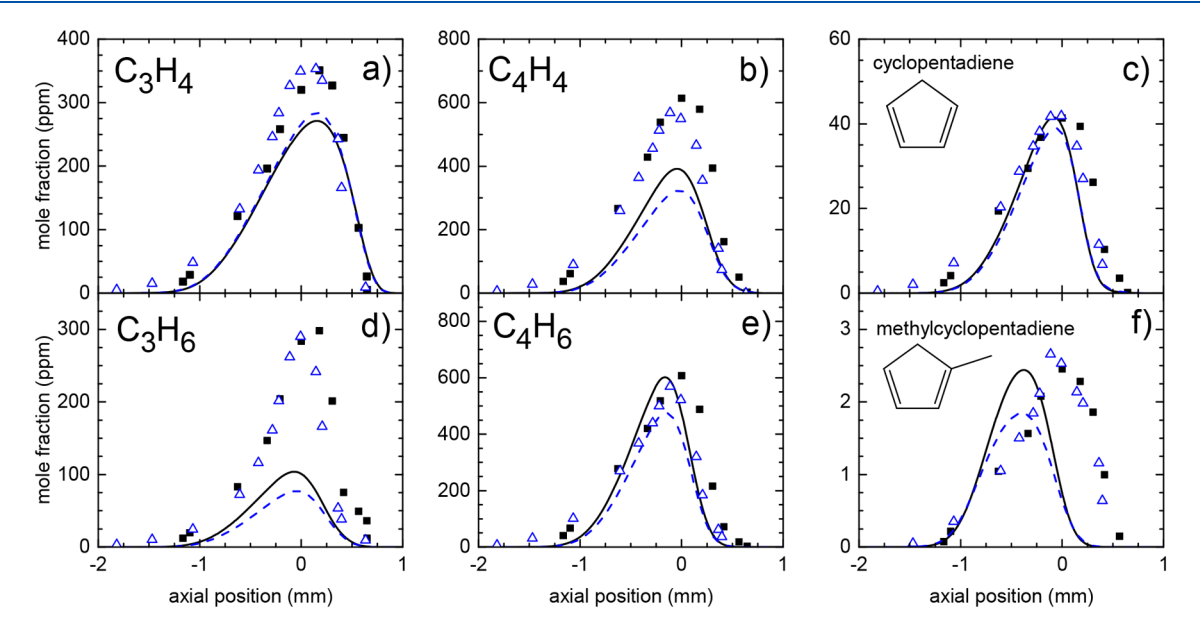


Figure 5. Mole fraction (ppm) profiles of critical C3-C5 species that are precursors to aromatic formation. Symbols and lines as in Figure 2.

the model predicts the cyclopentadienyl radical $(c\text{-}C_5\text{H}_5)$ to increase by ~50% in the toluene-seeded flame. The boost in cyclopentadienyl is from the benzyl radical and is predicted to contribute to aromatic formation via the aromatic radical recombination pathway. Indeed, the KM2 mechanism predicts a significant boost in the production of PAHs via aromatic radical recombination (e.g., indenyl + c-C5H5 \rightarrow phenanthrene +2H), but this pathway is still overshadowed by production via the classical HACA growth mechanism. There is a clear spatial offset (approximately 0.4 mm) between the experimental data and model profiles of methylcyclopentadiene (Figure 5f) whose origin is unclear. We can only rule out experimental error in the axial position because the experimental peak position of methylcyclopentadiene is consistent with that of all other species and any bias error in the experimental uncertainty would have been present in *all* species.

Figure 6 shows other aromatics and their increase with the addition of toluene that is, at least qualitatively, captured by the model: indene (Figure 6d) and methylnaphthalene (Figure 6b, lumped 2-methyl- and 1-methylnaphthalene) show a greater sensitivity, increasing by a factor of approximately 5 with toluene addition, whereas all other species increase by the factor of two to three, as was observed with benzene, naphthalene, and

phenanthrene in Figure 3. Methylnaphthalene is captured accurately only in the baseline flame, indicating that the model may be missing intermediates in a path from toluene to methylnaphthalene, which is otherwise dormant because of the low toluene mole fraction in the baseline ethylene flame. The dominant pathways leading to the formation of the remaining aromatic species in Figure 6 (styrene, acenaphthylene, biphenyl, and fluorene) are not affected by the addition of toluene fuel, and the increase in mole fraction appears to originate from the increase in the benzene mole fraction. Of course, production rates do increase with the addition of toluene, but the pathways are not altered, indicating that the formation of benzene remains the critical rate-limiting step to the production of these aromatic species.

There is an increase in aliphatic-linked PAHs in the toluene-seeded flame including biphenyl, diphenylmethane, bibenzyl, and diphenylacetylene, as shown in Figure 6. These PAHs are products of aromatic radical recombiantion and are intermediates in the cyclodehydrogenation mechanism leading to larger multiring aromatic species. ^{14,15,18,30,31} The last three of these species fall below the detection limit in the baseline flame, so the extent to which this pathway is enhanced with the addition of toluene is not quantified. While it appears that the

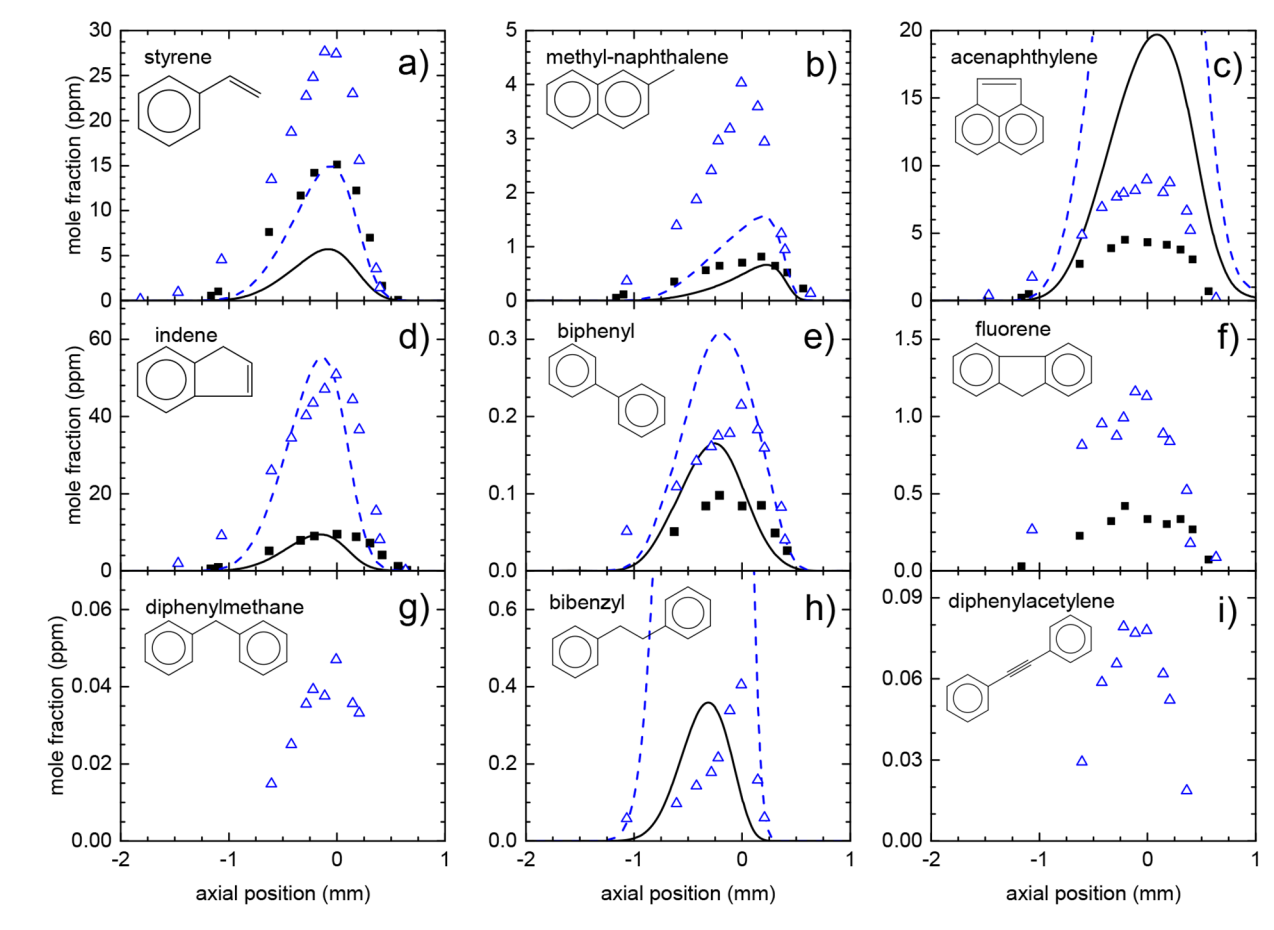


Figure 6. Mole fraction (ppm) profiles of other aromatic species. Symbols and lines as in Figure 2.

sequential growth of PAHs involving the HACA mechanism^{17,28,47,49} is the dominant pathway in both flames, the results of the toluene-seeded flame are consistent also with an aromatic radical recombination route 14,31 that may become the dominant pathway with higher toluene concentrations. Oddcarbon number species such as benzyl, cyclopentadienyl, and indenyl radicals were suggested to contribute to formation of PAHs^{16,31} such as naphthalene and phenanthrene (Figure 3). In the absence of quantitative data of radical concentrations, we can speculate that there should be an increase in benzyl and indenyl radicals because their stable counterparts, toluene and indene, increase in an appreciable amount in the toluene-seeded flame and are well predicted by the model. Cyclopentadienyl shows the lowest sensitivity to the addition of toluene among the oddcarbon species, indicating that the growth of the aromatic fuel is more favorable over the ring-opening of toluene or benzyl radical (e.g., benzyl \rightarrow c-C₅H₅ + C₂H₂). While these species appear in much lower concentrations than the three primary PAHs in Figure 3, the data in Figure 6 indicate there are new kinetic pathways that arise from the toluene fuel.

To highlight the difference in kinetic pathways between the two flames, a reaction path analysis tracking toluene ($C_6H_5CH_3$) pyrolysis was performed and is summarized in Figure 7. Species listed in bold are measured with GC/MS. A1, A2, and A4 are abbreviations for the number of aryl rings, representing benzene, naphthalene and pyrene, respectively. Starting with toluene that is highlighted in blue in the figure, we look at the reactions that result in net consumption (negative production rate) and follow the first few steps of the growth of intermediates to soot. For selected reactions, we report the primary collision partner and a

small table listing the percent of the total consumption for that particular partner in black for the baseline flame and in blue for the toluene-doped flame. In addition, we report the ratio of the integrated production rate for that particular path in the toluene flame to that of the baseline flame in green, to highlight which pathways are increased preferentially via toluene-doping. For less critical pathways, or for pathways where the percent of the total consumption remains constant for both baseline and toluene-doped flame, we report only the primary collision partner and the factor by which the integral of the production rate increased for the toluene-doped flame relative to the baseline. Consumption steps are denoted by black arrows. A few steps resulting in production of previously generated species are depicted by red arrows.

Toluene destruction and the subsequent growth to larger species is overwhelmingly by the H radical, with OH contributing a small percentage to the total production of benzyl radical (C₆H₅CH₂). Primary products of benzyl radical include indene (C₉H₈) and C₁₄H₁₄ (lumped isomers), with a small amount involving a ring opening mechanism to produce C2-C5 species. C2H2 (Figure 2) and C4H4 (Figure 5) mole fractions are nearly constant in both baseline and toluene-seeded flame, so the production of these aliphatic species is by the baseline ethylene fuel. The indene mole fraction is measured to increase by a factor of approximately 5 in the toluene-doped flame and is well captured by the model, which implies that the model represents accurately the acetylene addition to the benzyl radical increasing by an overall factor of 6.8 with the addition of toluene. Indene eventually leads to the production of pyrene (A4) and acenaphthylene (A2R5), after H radical attack to the

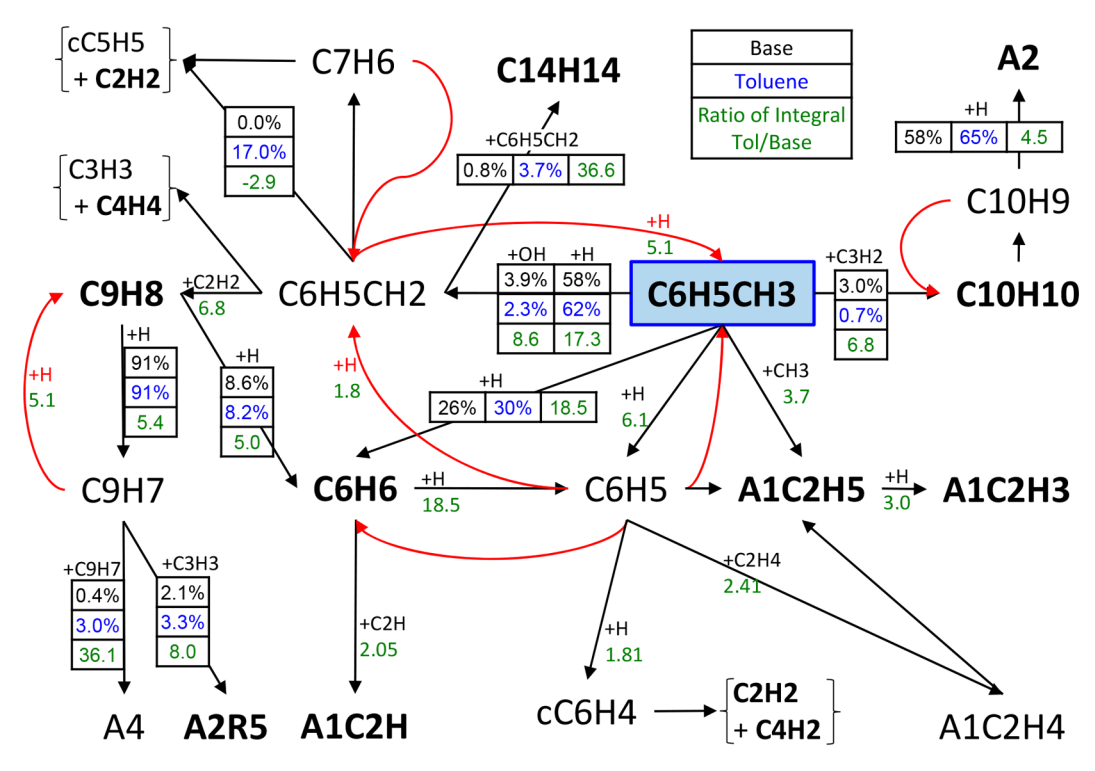


Figure 7. Reaction path analysis tracking toluene $(C_6H_5CH_3)$ pyrolysis. See text for interpretation.

indenyl radical, as shown in the lower left quadrant of Figure 7. Acenaphthylene is overpredicted by the model in both the baseline and toluene flame, but we observe in both experiments and model that the toluene-doped flame results in an increase in mole fraction relative to the baseline by a factor of approximate 2.5. Pyrene could not be measured with our GC/MS, but the model is predicting a 10-fold increase in mole fraction largely because of the increase in indene and indenvl radical (C_0H_7) in the toluene-doped flame. Pyrene was well captured in a similar baseline ethylene flame, 47 so there is some confidence that the model predictions are reasonably accurate, at least in the baseline flame, but subsequent studies can benefit from a quantification of pyrene to validate the indenyl radical dimerization rate constants. Similar to pyrene, C₁₄H₁₄ (e.g., bibenzyl; see Figure 6) is predicted to increase by a factor of approximately 10. This increase is solely due to the dimerization of the benzyl radical, but the model significantly overpredicts the experimental data so relevant rate constants may need to be

Benzene formation is one of the bottlenecks³⁶ to aromatic growth from an aliphatic parent fuel. So, it is worth looking closely at benzene formation and subsequent growth in the toluene flame. There is a significant increase in benzene production with toluene doping, and the model captures benzene well in both flames. In the toluene flame, the benzene mole fraction increases by a factor of two to three relative to the baseline flame (Figure 3), indicating that benzene is formed in comparable amounts from the baseline C₂H₄ fuel and toluene pyrolysis even though toluene is at significantly lower concentration. Thus, the benzene yield on a molar basis is roughly 2 orders of magnitude higher from toluene than ethylene. Benzene formation from toluene is predominantly by a direct H attack of toluene, with less than 5% coming from the enhanced indene pathway. The pathway from C₂H₄ to benzene is negligibly impacted with the addition of toluene, since the

molar fraction of aliphatic species (C5 and smaller) is identical in both baseline and toluene-doped flames. The subsequent growth from benzene remains relatively unaffected by the addition of toluene and products of toluene pyrolysis; i.e., the increase in mole fraction of phenylacetylene, styrene, ethylbenzene, and naphthalene (A1C₂H, A1C₂H₃, A1C₂H₅, and A2 in Figures 3 and 6 and the Supporting Information) in the toluene flame can largely be attributed to the original increase in the benzene mole fraction relative to the baseline flame.

In conclusion there appears to be two distinct pathways in the formation of larger aromatic species with toluene doping: a direct formation of benzene with subsequent aromatic growth by a sequential path via, for example, acetylene addition 18,47,50,51 , but also a radical recombination pathway with the production of $\rm C_{14}H_{14}$ (via dimerization of benzyl radical) and pyrene (through dimerization of indenyl radical).

Soot. Profiles of measured soot volume fraction and dispersion exponent of both flames are shown in Figure 8. Vertical lines mark the position of the flame front (right dashed line) and particle stagnation plane (left dash-dotted line); the latter is the location where the sum of the axial velocity and the thermophoretic velocity is zero. The thermophoretic velocity is calculated by $V_{th} = -0.538\nu\nabla \ln(T)$, so using the model to determine the temperature gradient and kinematic viscosity (ν) . Since the flame is on the oxidizer side of the gas stagnation plane, soot particles nucleating near the flame front and being convected away radially at the PSP have no opportunity to oxidize. The soot volume fraction profiles of both flames are qualitatively similar, but values for the toluene-seeded flame are approximately a factor of two larger than those of the baseline flame. This finding is not surprising in view of the marked increase in mole fraction of soot precursors (i.e., Figure 3), and the increase in radical recombination of aromatic species with methyl groups providing a pathway to larger PAHs that does not follow the traditional sequential growth. Near the PSP both the

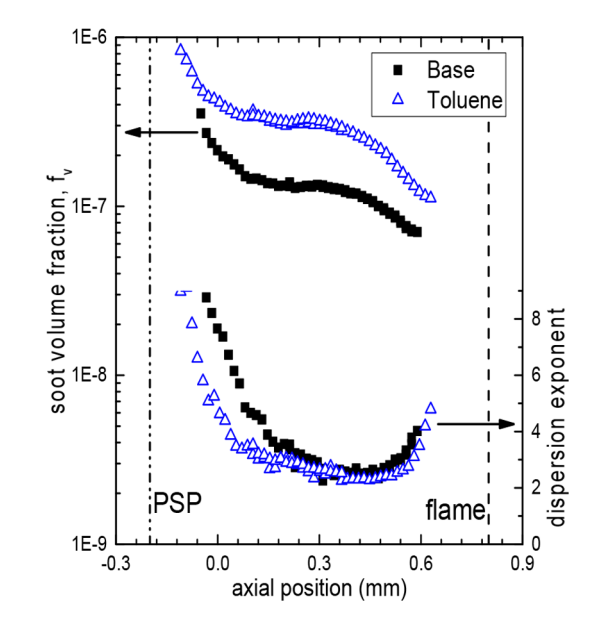


Figure 8. Soot volume fraction and dispersion exponent.

soot volume fraction and the dispersion exponent rise sharply, indicating that the particles H/C content increases and they are more transparent in the visible spectrum. A4,53 Particles dominated by PAHs or mixtures of PAHs and aliphatics can be transparent to visible light, A4 and small PAHs can be important for soot surface growth. The concentration of PAHs peak in proximity of the GSP, precisely where the increase in dispersion exponent occurs.

4. CONCLUSIONS

Detailed measurements in a toluene-doped atmospheric pressure counterflow diffusion flame of ethylene show unsurprisingly that replacing part of ethylene in the baseline flame with toluene results in a marked overall increase in soot formation. All aromatics increase by a factor of 2 or more with toluene doping, and the effect appears distributed through the entire soot laden region, consistent with the expectation that toluene pyrolysis leads readily to the formation of large PAHs and the formation of the first aromatic ring is no longer a bottleneck to soot formation. The subsequent growth from benzene remains relatively unaffected by the addition of toluene and products of toluene pyrolysis; i.e., the increase in mole fraction of phenylacetylene, styrene, ethylbenzene, and naphthalene in the toluene flame can largely be attributed to the increase in benzene mole fraction relative to the baseline flame. In addition, toluene doping bypasses completely benzene formation opening a radical recombination pathway to soot precursors through the production of C₁₄H₁₄ (via dimerization of benzyl radical) and pyrene (through dimerization of indenyl radical).

ASSOCIATED CONTENT

Supporting Information

The Supporting Information is available free of charge at https://pubs.acs.org/doi/10.1021/acs.jpca.2c06538.

Details of two-dimensional modeling and its effect on the computed temperature profile, mole fraction of all other measured species that are not shown in the main text (PDF)

AUTHOR INFORMATION

Corresponding Author

Alessandro Gomez — Department of Mechanical Engineering and Materials Science, Yale University, New Haven, Connecticut 06520-8286, United States; oorcid.org/0000-0003-2458-3370; Email: alessandro.gomez@yale.edu

Author

Kevin Gleason — Department of Mechanical Engineering and Materials Science, Yale University, New Haven, Connecticut 06520-8286, United States; Present Address: General Electric—Aerospace, 1 Neumann Way, Cincinnati, Ohio 45215, United States

Complete contact information is available at: https://pubs.acs.org/10.1021/acs.jpca.2c06538

Notes

The authors declare no competing financial interest.

ACKNOWLEDGMENTS

The authors acknowledge the support of the National Science Foundation (CBET-1853150).

REFERENCES

- (1) Edwards, T.; Maurice, L. Q. Surrogate Mixtures to Represent Complex Aviation and Rocket Fuels. *J. Propuls. Power* **2001**, *17* (2), 461–466
- (2) Pitz, W. J.; Mueller, C. J. Recent Progress in the Development of Diesel Surrogate Fuels. *Prog. Energy Combust. Sci.* **2011**, 37 (3), 330–350.
- (3) Honnet, S.; Seshadri, K.; Niemann, U.; Peters, N. A Surrogate Fuel for Kerosene. *Proc. Combust. Inst.* **2009**, 32, 485–492.
- (4) Dooley, S.; Won, S. H.; Chaos, M.; Heyne, J.; Ju, Y.; Dryer, F. L.; Kumar, K.; Sung, C. J.; Wang, H.; Oehlschlaeger, M. A.; Santoro, R. J.; Litzinger, T. A. A Jet Fuel Surrogate Formulated by Real Fuel Properties. *Combust. Flame* **2010**, *157* (12), 2333–2339.
- (5) Dooley, S.; Won, S. H.; Heyne, J.; Farouk, T. I.; Ju, Y.; Dryer, F. L.; Kumar, K.; Hui, X.; Sung, C. J.; Wang, H.; et al. The Experimental Evaluation of a Methodology for Surrogate Fuel Formulation to Emulate Gas Phase Combustion Kinetic Phenomena. *Combust. Flame* **2012**, *159* (4), 1444–1466.
- (6) Humer, S.; Frassoldati, A.; Granata, S.; Faravelli, T.; Ranzi, E.; Seiser, R.; Seshadri, K. Experimental and Kinetic Modeling Study of Combustion of JP-8, Its Surrogates and Reference Components in Laminar Nonpremixed Flows. *Proc. Combust. Inst.* **2007**, *31* (1), 393–400.
- (7) Witkowski, D.; Kondo, K.; Vishwanathan, G.; Rothamer, D. Evaluation of the Sooting Properties of Real Fuels and Their Commonly Used Surrogates in a Laminar Co-Flow Diffusion Flame. *Combust. Flame* **2013**, *160* (6), 1129–1141.
- (8) Dagaut, P.; Pengloan, G.; Ristori, A. Oxidation, Ignition and Combustion of Toluene: Experimental and Detailed Chemical Kinetic Modeling. *Phys. Chem. Chem. Phys.* **2002**, *4* (10), 1846–1854.
- (9) Yuan, W.; Li, Y.; Dagaut, P.; Yang, J.; Qi, F. Investigation on the Pyrolysis and Oxidation of Toluene over a Wide Range Conditions. II. A Comprehensive Kinetic Modeling Study. *Combust. Flame* **2015**, *162* (1), 22–40.
- (10) Won, S. H.; Dooley, S.; Dryer, F. L.; Ju, Y. Kinetic Effects of Aromatic Molecular Structures on Diffusion Flame Extinction. *Proc. Combust. Inst.* **2011**, 33 (1), 1163–1170.
- (11) Carbone, F.; Gomez, A. The Structure of Toluene-Doped Counterflow Gaseous Diffusion Flames. *Combust. Flame* **2012**, *159* (10), 3040–3055.
- (12) Carbone, F.; Gomez, A. Chemical Effects of 1,2,4-Trimethyl Benzene Addition in Counterflow Gaseous Diffusion Flames. *Proc. Combust. Inst.* **2013**, 34 (1), 1025–1033.

- (13) Choi, B. C.; Choi, S. K.; Chung, S. H. Soot Formation Characteristics of Gasoline Surrogate Fuels in Counterflow Diffusion Flames. *Proc. Combust. Inst.* **2011**, 33 (1), 609–616.
- (14) Hamins, A.; Anderson, D.; Miller, H. Mechanistic Studies of Toluene Destruction in Diffusion Flames. *Combust. Sci. Technol.* **1990**, 71 (4–6), 175–195.
- (15) Yuan, W.; Li, Y.; Dagaut, P.; Wang, Y.; Wang, Z.; Qi, F. A Comprehensive Experimental and Kinetic Modeling Study of N-Propylbenzene Combustion. *Combust. Flame* **2017**, *186*, 178–192.
- (16) Park, S.; Wang, Y.; Chung, S. H.; Sarathy, S. M. Compositional Effects on PAH and Soot Formation in Counterflow Diffusion Flames of Gasoline Surrogate Fuels. *Combust. Flame* **2017**, *178*, 46–60.
- (17) Mitra, T.; Zhang, T.; Sediako, A. D.; Thomson, M. J. Understanding the Formation and Growth of Polycyclic Aromatic Hydrocarbons (PAHs) and Young Soot from n-Dodecane in a Sooting Laminar Coflow Diffusion Flame. *Combust. Flame* **2019**, *202*, 33–42.
- (18) Mitra, T.; Chu, C.; Naseri, A.; Thomson, M. J. Polycyclic Aromatic Hydrocarbon Formation in a Flame of the Alkylated Aromatic Trimethylbenzene Compared to Those of the Alkane Dodecane. *Combust. Flame* **2021**, 223, 495–510.
- (19) Kruse, S.; Wick, A.; Medwell, P.; Attili, A.; Beeckmann, J.; Pitsch, H. Experimental and Numerical Study of Soot Formation in Counterflow Diffusion Flames of Gasoline Surrogate Components. *Combust. Flame* **2019**, *210*, 159–171.
- (20) Gu, M.; Liu, F.; Consalvi, J. L.; Gülder, Ö. L. Effects of Pressure on Soot Formation in Laminar Coflow Methane/Air Diffusion Flames Doped with n-Heptane and Toluene between 2 and 8 Atm. *Proc. Combust. Inst.* **2021**, 38, 1403–1412.
- (21) Chu, C.; Zhang, T.; Thomson, M. J. The Chemical Structure Effects of Alkylbenzenes on Soot Formation in a Laminar Co-Flow Flame. *Combust. Flame* **2019**, 204, 237–249.
- (22) Choi, S. K.; Choi, B. C.; Lee, S. M.; Choi, J. H. The Effect of Liquid Fuel Doping on PAH and Soot Formation in Counterflow Ethylene Diffusion Flames. *Exp. Therm. Fluid Sci.* **2015**, *60*, 123–131.
- (23) Jahangirian, S.; McEnally, C. S.; Gomez, A. Experimental Study of Ethylene Counterflow Diffusion Flames Perturbed by Trace Amounts of Jet Fuel and Jet Fuel Surrogates under Incipiently Sooting Conditions. *Combust. Flame* **2009**, *156* (9), 1799–1809.
- (24) Daca, A. E.; Gülder, Ö. L. Soot Formation Characteristics of Diffusion Flames of Methane Doped with Toluene and N-Heptane at Elevated Pressures. *Proc. Combust. Inst.* **2017**, *36* (1), 737–744.
- (25) Bufferand, H.; Tosatto, L.; La Mantia, B.; Smooke, M. D.; Gomez, A. Experimental and Computational Study of Methane Counterflow Diffusion Flames Perturbed by Trace Amounts of Either Jet Fuel or a 6-Component Surrogate under Non-Sooting Conditions. *Combust. Flame* **2009**, *156* (8), 1594–1603.
- (26) McEnally, C. S.; Pfefferle, L. D.; Atakan, B.; Kohse-Hoinghaus, K. Studies of Aromatic Hydrocarbon Formation Mechanisms in Flames: Progress towards Closing the Fuel Gap. *Prog. Energy Combust. Sci.* **2006**, 32 (3), 247–294.
- (27) Valencia-López, A. M.; Bustamante, F.; Loukou, A.; Stelzner, B.; Trimis, D.; Frenklach, M.; Slavinskaya, N. A. Effect of Benzene Doping on Soot Precursors Formation in Non-Premixed Flames of Producer Gas (PG). *Combust. Flame* **2019**, 207, 265–280.
- (28) Frenklach, M.; Wang, H. Detailed Modeling of Soot Particle Nucleation and Growth. *Proc. Combust. Inst.* **1991**, 23 (1), 1559–1566.
- (29) Matsugi, A.; Miyoshi, A. Modeling of Two- and Three-Ring Aromatics Formation in the Pyrolysis of Toluene. *Proc. Combust. Inst.* **2013**, 34 (1), 269–277.
- (30) Sinha, S.; Raj, A. Polycyclic Aromatic Hydrocarbon (PAH) Formation from Benzyl Radicals: A Reaction Kinetics Study. *Phys. Chem. Chem. Phys.* **2016**, *18* (11), 8120–8131.
- (31) Johansson, K. O.; Lai, J. Y. W.; Skeen, S. A.; Popolan-Vaida, D. M.; Wilson, K. R.; Hansen, N.; Violi, A.; Michelsen, H. A. Soot Precursor Formation and Limitations of the Stabilomer Grid. *Proc. Combust. Inst.* **2015**, 35 (2), 1819–1826.
- (32) Johansson, K. O.; Head-Gordon, M. P.; Schrader, P. E.; Wilson, K. R.; Michelsen, H. A. Resonance-Stabilized Hydrocarbon-Radical

- Chain Reactions May Explain Soot Inception and Growth. *Science*. **2018**, *361* (6406), 997–1000.
- (33) Wang, Y.; Chung, S. H. Soot Formation in Laminar Counterflow Flames. *Prog. Energy Combust. Sci.* **2019**, 74, 152–238.
- (34) Gleason, K.; Carbone, F.; Gomez, A. Pressure and Temperature Dependence of Soot in Highly Controlled Counterflow Ethylene Diffusion Flames. *Proc. Combust. Inst.* **2019**, 37 (2), 2057–2064.
- (35) Gleason, K.; Carbone, F.; Gomez, A. Effect of Temperature on Soot Inception in Highly Controlled Counterflow Ethylene Diffusion Flames. *Combust. Flame* **2018**, *192*, 283–294.
- (36) Wang, H. Formation of Nascent Soot and Other Condensed-Phase Materials in Flames. *Proc. Combust. Inst.* **2011**, 33 (1), 41–67.
- (37) Anderson, H.; McEnally, C. S.; Pfefferle, L. D. Experimental Study of Naphthalene Formation Pathways in Non-Premixed Methane Flames Doped with Alkylbenzenes. *Proc. Combust. Inst.* **2000**, 28 (2), 2577–2583.
- (38) Figura, L.; Carbone, F.; Gomez, A. Challenges and Artifacts of Probing High-Pressure Counterflow Laminar Diffusion Flames. *Proc. Combust. Inst.* **2015**, 35 (2), 1871–1878.
- (39) Today in Energyhttps://www.eia.gov/todayinenergy/detail.php?Id=41433 (accessed March 28, 2022).
- (40) International Energy Outlook 2021. https://www.eia.gov/outlooks/ieo/ (accessed March 28, 2022).
- (41) Figura, L.; Gomez, A. Structure of Incipiently Sooting Ethylene-Nitrogen Counterflow Diffusion Flames at High Pressures. *Combust. Flame* **2014**, *161* (6), 1587–1603.
- (42) Andrews, G. E.; Bradley, D.; Hundy, G. F. Hot Wire Anemometer Calibration for Measurements of Small Gas Velocities. *Int. J. Heat Mass Transfer* **1972**, *15* (10), 1765–1786.
- (43) Kuhn, P. B.; Ma, B.; Connelly, B. C.; Smooke, M. D.; Long, M. B. Soot and Thin-Filament Pyrometry Using a Color Digital Camera. *Proc. Combust. Inst.* **2011**, 33 (1), 743–750.
- (44) D'Anna, A. Combustion-Formed Nanoparticles. *Proc. Combust. Inst.* 2009, 32 (1), 593–613.
- (45) CHEMKIN-ProRelease R2; ANSYS, 2019.
- (46) Wang, Y.; Raj, A.; Chung, S. H. A PAH Growth Mechanism and Synergistic Effect on PAH Formation in Counterflow Diffusion Flames. *Combust. Flame* **2013**, *160* (9), *1667*–1676.
- (47) Gleason, K.; Carbone, F.; Sumner, A. J.; Drollette, B. D.; Plata, D. L.; Gomez, A. Small Aromatic Hydrocarbons Control the Onset of Soot Nucleation. *Combust. Flame* **2021**, 223, 398–406.
- (48) Carbone, F.; Cattaneo, F.; Gomez, A. Structure of Incipiently Sooting Partially Premixed Ethylene Counterflow Flames. *Combust. Flame* **2015**, *162* (11), 4138–4148.
- (49) Mitra, T.; Amidpour, Y.; Chu, C.; Eaves, N. A.; Thomson, M. J. On the Growth of Polycyclic Aromatic Hydrocarbons (PAHs) in a Coflow Diffusion Flame of Ethylene. *Proc. Combust. Inst.* **2021**, *38*, 1507–1515.
- (50) Frenklach, M.; Clary, D. W.; Gardiner, W. C.; Stein, S. E. Detailed Kinetic Modeling of Soot Formation in Shock-Tube Pyrolysis of Acetylene. *Proc. Combust. Inst.* **1985**, *20* (1), 887–901.
- (51) Houston Miller, J.; Smyth, K. C.; Mallard, W. G. Calculations of the Dimerization of Aromatic Hydrocarbons: Implications for Soot Formation. *Proc. Combust. Inst.* **1985**, *20* (1), 1139–1147.
- (52) Waldmann, L.; Schmitt, K. H. Thermophoresis and Diffusiophoresis of Aerosols. *Aerosol Sci.* **1966**, *137*, 163–194.
- (53) Russo, C.; Apicella, B.; Tregrossi, A.; Ciajolo, A.; Le, K. C.; Török, S.; Bengtsson, P. E. Optical Band Gap Analysis of Soot and Organic Carbon in Premixed Ethylene Flames: Comparison of in-Situ and Ex-Situ Absorption Measurements. *Carbon N. Y.* **2020**, *158*, 89–96.
- (54) Cain, J.; Laskin, A.; Kholghy, M. R.; Thomson, M. J.; Wang, H. Molecular Characterization of Organic Content of Soot along the Centerline of a Coflow Diffusion Flame. *Phys. Chem. Chem. Phys.* **2014**, 16 (47), 25862–25875.
- (55) Kholghy, M. R.; Kelesidis, G. A.; Pratsinis, S. E. Reactive Polycyclic Aromatic Hydrocarbon Dimerization Drives Soot Nucleation. *Phys. Chem. Chem. Phys.* **2018**, 20 (16), 10926–10938.